Shallow impurities and δ-doping in quantum dot–quantum well systems

2001 J. Phys.: Condens. Matter 13 8105

(http://iopscience.iop.org/0953-8984/13/35/316)

INSTITUTE OF PHYSICS PUBLISHING JOURNAL OF PHYSICS: CONDENSED MATTER

J. Phys.: Condens. Matter **13** (2001) 8105–8119 PII: S0953-8984(01)23969-1

Shallow impurities and δ-doping in quantum dot–quantum well systems

V Ranjan and Vijay A Singh

Physics Department, IIT, Kanpur, UP-208016, India

Received 18 April 2001
Published 16 August 2001
Online at stacks.iop.org/JPhysCM/13/8105

Abstract

In the present work we study the defect states in recently synthesized semiconductor quantum dot–quantum well systems (QDQWs). We employ the effective-mass theory (EMT) with a realistic barrier and variable effective mass. The model is simple and all of our results are obtained by an exact numerical diagonalization of the Schrödinger equation. We study the ground state of the host system as a function of quantum well size. We demonstrate that the upshift with QDQW downsizing differs from reported upshifts in simple quantum dots (QDs) and explain this by means of a perturbative analysis. We study the binding energy of the hydrogenic impurity and its variation with QDQW size. Next the binding energy is studied as the impurity is moved off-centre. We find that the binding energy goes through a maximum. An analysis of the wavefunction is carried out to obtain an understanding of this surprising effect. The impurity calculations are carried out on CdS/HgS/CdS QDQWs. Recently, experimental studies on a monolayer of HgS in a CdS dot were carried out. We model this system as a 'δ-defect' consisting of a thin spherical shell of fixed potential depth in a spherical CdS dot. The ground state of this system is studied as the shell is dragged from the periphery to the centre of the CdS dot. Our results are explained on the basis of qualitative arguments and asymptotic analyses. Outstanding issues and future directions are suggested.

1. Introduction

Semiconductor nanocrystallites, more popularly known as quantum dots (QDs), have been studied for over two decades. The system is interesting from the point of view of basic physics since the carriers are confined to an essentially 'zero'-dimensional structure. The efficient luminescence observed in some of these crystallites makes them promising candidates for use in opto-electronic devices. Further, the inexorable drive towards smaller and ever smaller devices makes them technologically significant. Besides the size miniaturization, surface effects are also known to influence the optical properties of these nanometre particles [1]. To

suppress surface effects, inorganic passivation has been utilized where the nanocrystals have been covered with a high-band-gap material [2]. Such a system, known as a quantum dot–quantum well system (QDQW), has more efficient fluorescence. The study of impurity states in low-dimensional heterostructures is technologically important. There are many theoretical and experimental works devoted to study of defect states in QDs but there are hardly any studies of defects in QDQWs. In this paper we aim to study some interesting features of QDQWs and, mainly, the properties of defect states in them.

We first briefly survey the field of impurity states in QDs. The study of impurity states in low-dimensional heterostructures is an important aspect, to which many theoretical and experimental works have been devoted. Experimental work in connection with impurities in semiconductor nanostructures is preliminary and is of recent origin [3–5]. The first calculations on the binding energy of hydrogenic impurities in a quantum well were reported by Bastard [6]. He found that the binding energy depends both on the position of the impurity and on the well thickness. This work was followed by several others [7, 8]. The past two decades have witnessed several developments in the synthesis of quantum dots (QDs). This attracted the attention of some workers towards hydrogenic impurities in QDs. Zhu compared calculations for the binding energy of the hydrogenic impurity in a QD with that in the two-dimensional quantum well. He found that the binding energy is larger in a QD [9]. Chuu *et al* [10] reported the hydrogenic impurity states in quantum dots and quantum wires using an exact solution of the Hamiltonian. Porras-Montenegro and Perez-Merchancano [11] studied the hydrogenic impurity in QDs. Theirs was a variational calculation for impurities in $GaAs/Al_{1-x}Ga_xAs$. The same group later reported the density of states of the impurity [12]. Ribeiro and Latge [13] compared the same for the cubic dots with that for a spherical QD. They also studied the effect of dimensionality and shape of quantum dots. Zhu *et al* have also reported the D^0 and D^- donor states in a QD [14]. The effect of intense laser field on hydrogenic impurities in quantum dots was studied by Fanyao *et al* [15]. They found that the intense field effectively shifts the impurity from the centre of the QD to some off-centre position. In a recent work Zhu *et al* [16] have investigated the influence of dot size and potential shape on the binding energy for a hydrogenic impurity in a quantum dot. Charrour *et al* have investigated the effect of magnetopolarons in cylindrical quantum dots [17]. In a detailed analysis carried out recently, we [18] have shown that the binding energy of the impurity undergoes a shallow-to-deep (SHADE) transition as the dot size is reduced. In other words a nominally shallow level in the bulk is likely to become deep in the QD. If, further, one takes into account the dependence of the dielectric constant on the size ($\epsilon = \epsilon(R)$), then the binding energy becomes deeper still. Thus there is every likelihood of carrier 'freeze-out' [18]. The work in this field is still continuing and our references above are only representative. Finally we note that the confined hydrogen atom has been studied as an academic curiosity for quite some time [19].

The field of QDQWs is nascent. A QDQW is a heterostructure, composed of two different semiconductor materials. Eychmüller and co-workers [20, 21] were the first to synthesize QDQWs. The wet chemical synthesis, the characterization, and some linear and non-linear optical properties of QDQWs have recently been reported in detail [20, 21]. It has been shown that the linear absorption of QDQWs differs significantly from that of the constituent materials. The band gap can be tuned by core diameter and the well thickness. Haus *et al* [22] showed that the band gap of the composite material depends on both the core and shell radii. Effective-mass theory (EMT) has been used to successfully describe the electronic properties of this system [23–26]. To the best of our knowledge no work on an impurity in a QDQW system has been reported.

In the next section (section 2) we explain the model that we have developed for QDQWs and sketch the basic theory that we have adopted in achieving this task. Similar models were

discussed earlier in the literature and this brief discussion on the model is included here for the sake of completeness and to establish our notation. We discuss the behaviour of a QDQW host, i.e. a QDQW without impurity. We find that the ground-state energy of a QDQW decreases as the well thickness (HgS layer thickness) is increased for a given dot (the inner CdS core) size. However, the gradient of the ground-state energy versus QDQW size curve is at variance with that for a bare quantum dot. We explain this behaviour by means of a perturbative analysis.

In section 3 we present our calculation for defect states in a QDQW. We have performed calculations for the hydrogenic impurity at the centre of a QDQW and find that the binding energy increases monotonically as the well size is decreased for a given dot size. Next the hydrogenic impurity is shifted off-centre, and we find that first, the binding energy increases monotonically and then, after attaining a maximum, it starts decreasing for given dot and well sizes. We can explain this surprising feature by examining the wavefunction and by simple qualitative arguments. Finally we calculate the ground-state energy of the CdS/HgS system with the HgS layer being grown within the CdS QD at different positions between the surface and the centre of the QD. The HgS consists of a single monolayer and the system may be viewed as a thin spherical defect shell in a spherical CdS host. This is reminiscent of a delta-doped semiconductor system [27]. We label this exotic arrangement a 'δ-defect' system. Some of our results are compared with recently reported experiments [2]. We also explain the results on the basis of perturbative and asymptotic analyses.

The last section (section 4) encapsulates our conclusions. Experimental tests for our work and future directions for research are indicated.

2. Host QDQWs

We consider a spherical semiconductor nanocrystallite heterostructure of dot size $d = 2R$ (see figure 1). We study the effect on impurity level of the finite size of the nanocrystallite. The defect in our model is at the origin, i.e. at the centre of the nanocrystallite (figure 1). The Hamiltonian of the hydrogenic level in such a crystallite is described in effective-mass theory by the following equation:

$$H = -\frac{\hbar^2}{2}\vec{\nabla}\cdot\left(\frac{1}{m^*(\vec{r})}\vec{\nabla}\right) - \frac{e^2}{\epsilon r} + V(\vec{r}). \tag{2.1}$$

For a position-dependent mass the appropriate Hermitian kinetic energy operator is given by the first term on the right-hand side of equation (2.1) [28]. The nanocrystallite consists of several layers of different materials. The core of such heterostructures is called the quantum dot (QD) and the several layers of shells covering the QD are called quantum wells (QWs). The electron effective masses in different layers are different as they consist of different materials. The electron effective mass inside the QD (m_i) is different from the effective mass in the shell (m_o). It is useful to define a parameter, β, which is the ratio of the effective masses:

$$\beta = \frac{m_i}{m_o}. \tag{2.2}$$

The second term in the Hamiltonian is the impurity potential, where e is the charge on an electron and ϵ is the relative dielectric constant of the material. In figure 1 the appropriate potential for describing the QDQW is depicted. From left to right one sees the core (QD) for $r \leqslant R_d$, the first shell (well 1) for $R_d \leqslant r \leqslant R_{w1}$, and well 2 for $R_{w1} \leqslant r \leqslant R_{w2}$. The exact values of these potentials depend on the band offset, i.e. the difference between the conduction band minima of the two different materials. The potential $V(r)$ in equation (2.1) is given by

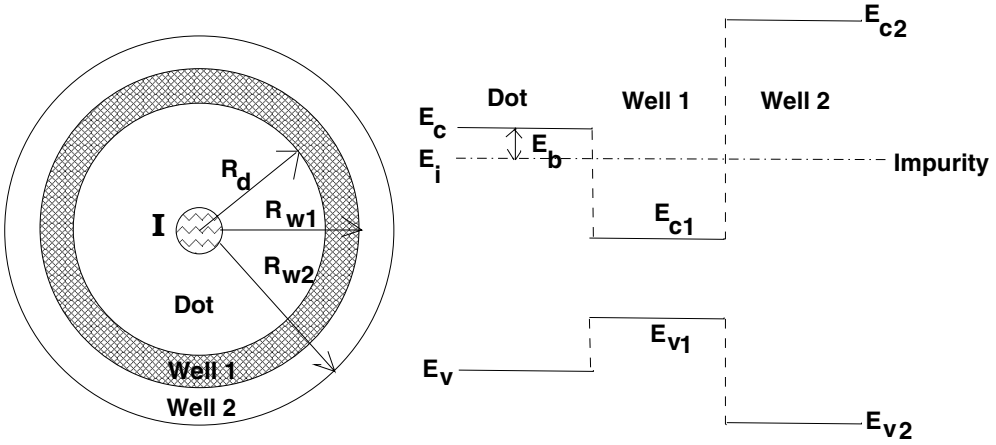

Figure 1. The left-hand side of the figure depicts a spherical quantum dot–quantum well system (QDQW). In the figure we have shown three layers of material. In general there can be any number of layers of different materials. The inner core is called the quantum dot and the shell surrounding the inner core is like a quantum well. Here in this figure we have shown a dot surrounded by two wells, well 1 and well 2. The dot radius is R_d and the radius of the heterostructure up to the first well is R_{w1}, and up to the second well is R_{w2}. There is an impurity at the centre of this heterostructure. We have represented it by **I** in this figure. On the right-hand side of the figure we have modelled the heterostructure by a potential diagram. The conduction band minima (CBM) and valence band maxima (VBM) of the dot, well 1, and well 2 are shown in the diagram. We can see in the diagram that there is a conduction band offset for different layers. The impurity level is shown bound to the conduction band minima by a small binding energy.

$$V(r) = \begin{cases} V_1 & r \leqslant R_d \\ 0 & R_d \leqslant r \leqslant R_{w1} \\ V_2 & R_{w1} \leqslant r \leqslant R_{w2}. \end{cases} \tag{2.3}$$

Here V_2 is a large positive potential and represents the dielectric coating surrounding the nanocrystallite. Typically a nanocrystallite is surrounded by dielectrics such as glasses, polymers, organic solvents, or oxides and hydrides [29]. The electron is in a spherically symmetric well.

As mentioned earlier, the electron effective mass m^* assumes different values in different layers of the heterostructures. Contrary to the suggestions made in standard quantum mechanics textbooks regarding the continuity of the first derivative of the wavefunction across the boundary, we apply the BenDaniel–Duke [28] boundary condition for the heterostructures under study. The condition now reads

$$\frac{1}{m_i}\frac{\mathrm{d}R_{nl}}{\mathrm{d}r}\bigg|_{r\to R^-} = \frac{1}{m_o}\frac{\mathrm{d}R_{nl}}{\mathrm{d}r}\bigg|_{r\to R^+}. \tag{2.4}$$

As demonstrated in a previous work [1], a point of some significance is the issue of applying the boundary condition to the partial wavefunction or the full wavefunction. It is shown there that applying the boundary condition to the partial wavefunction is manifestly incorrect when we use the modified boundary condition. In the above equation (equation (2.4)) R_{nl} is the full wavefunction. The partial wavefunction is given by $u_{nl}(r) = rR_{nl}$. Here we have used the full wavefunction in all our calculations. In the above paragraphs we have explained a general framework within which we can define a nanostructure heterostructure, sometimes called a

heteronanostructure for short. We have used this model to study the host QDQW and defect states in the QDQW.

We have carried out calculations for the ground-state energy of a carrier in a QDQW. Such systems have generated a lot of interest in recent times. The model that we have used for this calculation has been defined in section 2. We have solved the Hamiltonian (equation (2.1)) numerically (see appendix A) on a grid, using the Runge–Kutta–Fehlberg method. We have adopted a finer mesh near the potential discontinuity. The program consistently provides both fast and stable results. We have cross-checked our results with the predictor–corrector approach. The Hamiltonian in equation (2.1) without the impurity potential term is used to solve this problem. We have solved our problem for the electron ground state. In regions where $E_{nl} > V_q$, the solution of the Schrödinger equation, equation (2.1), is given in terms of well known spherical Bessel and Neumann functions j_l and n_l:

$$R_{nl,q} = A_{nl,q}\, j_l(k_{nl,q}r) + B_{nl,q}\, n_l(k_{nl,q}r) \tag{2.5}$$

with

$$k_{nl,q} = \sqrt{\frac{2m_q^*(E_{nl} - V_q)}{\hbar^2}}. \tag{2.6}$$

V_q is the value of $V(r)$ in different layers of the QDQW as defined in equation (2.3), q denoting different layers of the QDQW, and m_q is the effective mass of an electron in region q. E_{nl} is the CBM energy.

In regions where $E_{nl} < V_q$, the solution is a linear combination of two Hankel functions $h_l^{(+)}$ and $h_l^{(-)}$:

$$R_{nl,q} = C_{nl,q}\, h_l^{(+)}(\mathrm{i}\kappa_{nl,q}r) + D_{nl,q}\, h_l^{(-)}(\mathrm{i}\kappa_{nl,q}r) \tag{2.7}$$

with

$$\kappa_{nl,q} = \sqrt{\frac{2m_q^*(V_q - E_{nl})}{\hbar^2}}. \tag{2.8}$$

A, B, C, and D are constants.

A word on the nomenclature. We have used the term 'conduction band minimum (CBM)' and the 'ground state of the carrier' in a QDQW interchangeably. Recognizing the discrete nature of the energy spectra in a QD, many workers have termed this state the lowest unoccupied molecular orbital (LUMO) or simply the ground state. However, the term conduction band is also employed in this field [30, 31]. Moreover, the use of bulk-related terms such as 'gap', 'band', and 'CBM' is fairly common in the field of QDQWs [22, 23, 25, 26].

We have performed our calculations for the CdS core and HgS shell surrounded by a dielectric medium. The effective mass of the electron is taken to be 0.2 m_e and 0.036 m_e in CdS and HgS, respectively. The dielectric constant is taken as 5.5 and 11.36 respectively for CdS and HgS. The bulk band gap of CdS is 2.5 eV and that of HgS is 0.5 eV. The conduction band offset is 1.35 eV. Hence the value of V_1 in equation (2.3) is 1.35 eV. In the dielectric medium we have taken the electron effective mass to be the free-electron mass (m_e) and the dielectric constant to be unity. The above-mentioned parameters have been taken from Chang and Xia [24].

The ground-state energy of the QDQW is plotted as a function of core and shell radii in figure 2. Each curve in the figure is for a fixed core radius (R_d), i.e. a fixed dot size, and varying radii of the QDQW (R_w), i.e. varying well sizes. The solid line on the extreme right is for the largest CdS dot radius that we have considered. The QD radius here is 23.5 Å. The dashed line on the extreme left in the figure is for the smallest dot radius that we have considered.

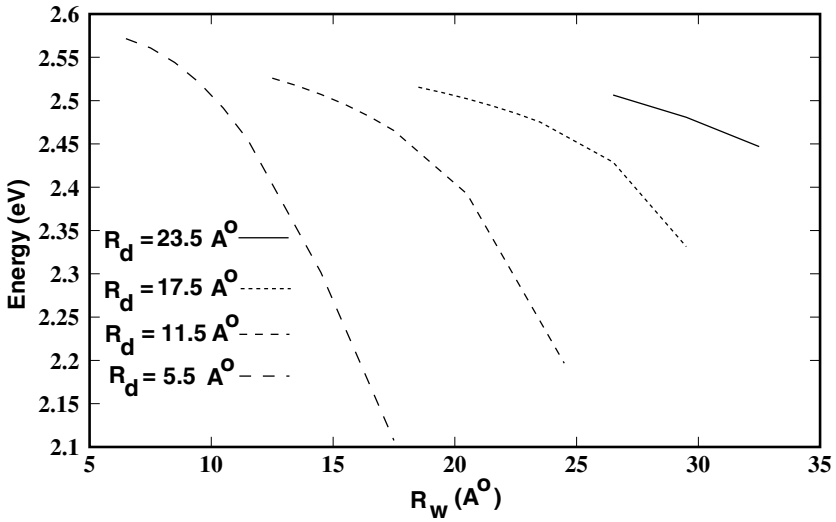

Figure 2. This plot shows the conduction band minima as functions of the CdS/HgS QDQW radius R_w. Here R_d is the radius of the dot (see figure 1). Each curve is for a fixed dot radius but varying well thickness. As the well size is increased the CBM lowers, in conformity with the quantum confinement model. However, the curvature of each of these curves is opposite to that for a single dot.

The QD radius here is 5.5 Å. For each of these QD sizes (R_d) we have done calculations for well thicknesses $\Delta(=R_w - R_d)$ varying from 1 Å to 12 Å. As the well thickness is reduced from 12 Å to 1 Å we see that the CBM for the QDQW increases and becomes equal to the CBM for the QD of the relevant size.

If we compare the trend of rising ground-state energy with that of the ground-state energy for simple quantum dots [1], we find that the curvatures for these are opposite to each other. The ground state rises with a steep slope at small QD size for a quantum dot. On the other hand, when the well size is reduced to zero, the ground state of a QDQW approaches that of a QD asymptotically with almost zero slope as seen in figure 2. This may explain the difference in curvature between the two cases, QD and QDQW, and hence the incumbent trend for the rise in energy.

It would be interesting to verify this trend experimentally. There appears to be some indirect evidence for it. Mews *et al* [21] have charted the 1s–1s transition (CBM to VBM) of a CdS/HgS/CdS QDQW with varying HgS layer thickness. These experiments could be extended to verify our prediction.

We also adopt a perturbative approach to explain this trend in a QDQW. We assume that the entire QDQW is composed of CdS only. Hence we solve for the ground-state energy E of a CdS QD of size R_w surrounded by a dielectric. As is known from quantum confinement [1],

$$E \approx C/R_w^{\gamma} \tag{2.9}$$

where C is a constant and the exponent γ is between 1 and 2. Hence

$$\frac{\mathrm{d}E}{\mathrm{d}R} = \frac{-C\gamma}{R_w^{\gamma+1}}.$$

Thus the ground-state energy rises steeply with a negative slope at small R_w. Next we introduce a perturbation V_p $(=-V_1)$ of thickness Δ $(= R_w - R_d)$ at the edge of CdS QD of size R_w. In

this region of perturbation we use all the parameters (effective mass, dielectric constant, etc) of HgS described above. This is equivalent to taking the HgS layer as a perturbation to a CdS inner core. The perturbation Hamiltonian which is defined over the range $r \in [R_d, R_w]$ can be written, in atomic units ($\hbar = 1, m_e = 1/2$), as

$$H_p = \left[\frac{1}{m_1^*} - \frac{1}{m_2^*}\right]\frac{\mathrm{d}^2}{\mathrm{d}r^2} + V_p \tag{2.10}$$

$$E_p = 4\pi A^2\left[\frac{k^2}{\mu} + V_p\right]\int_{R-d}^{R_w} \sin^2(kr)\,\mathrm{d}r \tag{2.11}$$

where m_1^* and m_2^* are the effective masses of the electron in the CdS and HgS layers, respectively. We solve this problem in the limit of an infinite barrier provided by the dielectric coating. If we assume the sinusoidal form for the ground-state wavefunction for a carrier inside the CdS QD, then the perturbative energy (E_p) is given in atomic units by

$$E_p = 4\pi A^2\left[\frac{k^2}{\mu} + V_p\right]\left[\frac{\Delta}{2} - \frac{\sin(2kR_w) - \sin(2kR_d)}{4k}\right] \tag{2.12}$$

where $1/\mu = 1/m_2^* - 1/m_1^*$ and $k^2 = m_1^* E$, and E is given by equation (2.9). For the case under consideration, μ is positive. In the above equation, A is the normalization constant for the wavefunction in a QD. In the limit of an infinite barrier, the quantities described above approach the following limits: $A^2 \to 1/(2\pi R_w)$, $k \to \pi/R_w \Rightarrow \sin(2kR_w) \to 0$. Hence,

$$E_p = \frac{2}{R_w}\left[\frac{\pi^2}{\mu R_w^2} + V_p\right]\left[\frac{\Delta}{2} + \frac{\sin(2kR_d)}{4k}\right]. \tag{2.13}$$

In the limit of small $\Delta (R_w \sim R_d)$, $k\Delta \ll 1$,

$$\sin(2kR_d) = \sin(2k(R_w - \Delta)) \approx -\sin(2k\Delta) = -(2k\Delta) + \frac{(2k\Delta)^3}{6} + \cdots. \tag{2.14}$$

The ground-state energy (CBM) of the CdS/HgS QDQW will be given by the sum of $E(=C/R_w^\gamma)$ and the perturbative energy E_p. We need to examine the dependence of E_p on Δ since the unperturbed part does not explicitly depend on Δ. Hence,

$$\begin{aligned} &E_p \approx \frac{2}{R_w}\left[\frac{\pi^2}{\mu R_w^2} + V_p\right]\left(\frac{1}{3}\frac{\pi^2}{R_d^2}\right)\Delta^3 \\ &\frac{\partial E_p}{\partial \Delta} \to 0 \qquad \text{as } \Delta \to 0. \end{aligned} \tag{2.15}$$

The assumption of small $k\Delta$ implies that R_w is close to R_d. Using $k \to \pi/R_w$, we obtain $R_d < R_w < 1.4R_d$. The expression within the square brackets is dominated by $V_p = -V_1$ and is, hence, negative for large R_w. To be more specific, $R_w > \pi/\sqrt{\mu V_1}$. For the parameters under consideration, the above asymptotic analysis holds if $R_w \geqslant 20$ Å. Thus equation (2.15) shows that in the limit of well thickness approaching zero, we get the expected behaviour as depicted in figure 2.

3. Defects in QDQWs

In this section we report calculations for defect states in a QDQW. We have completed this exercise for three different types of defect: (i) on-centre hydrogenic impurities; (ii) off-centre hydrogenic impurities; and (iii) δ-defects in a quantum dot. The aim is to calculate the binding

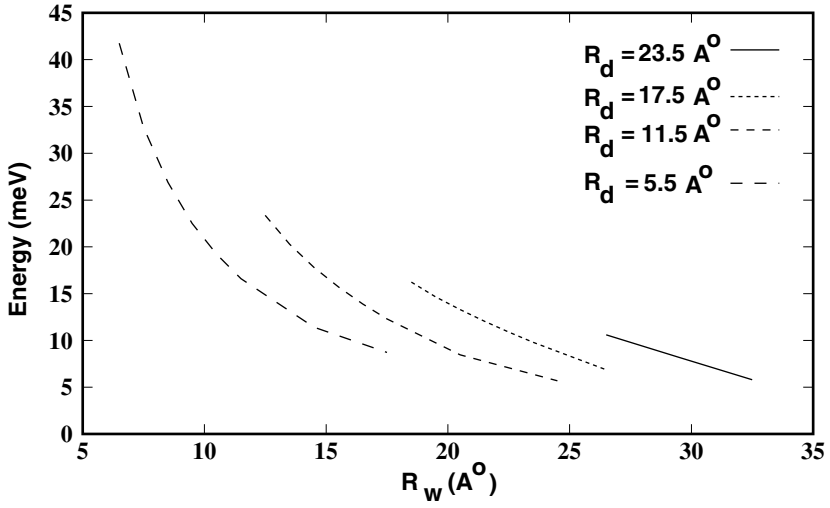

Figure 3. This plot shows the binding energy of an impurity at the centre of the CdS/HgS QDQW as a function of QDQW radius R_w. Here R_d is the radius of the dot (see figure 1). Each curve is for a fixed dot radius but varying well thickness. We can see that the defect level gets deeper as the well thickness is lowered. Here we do not observe any shallow–deep (SHADE) transition.

energy of these systems, and to provide explanations and possible experimental tests. The impurity binding energy (E_b) defined as

$$E_b = E_c - E_i \tag{3.1}$$

is the difference between the CBM level of the host (E_c) and the impurity level (E_i).

First we perform calculations for the binding energy of a hydrogenic impurity at the centre of the QDQW. The sizes of the core and shell are the same as for the calculation of the ground-state energy (E_c) of the QDQW described in the previous section.

We have solved the Hamiltonian (equation (2.1)) numerically (see appendix A). The method of solution is similar to the one described in section 2. We have included the complete Hamiltonian with the impurity potential, equation (2.1), to solve this problem. These calculations have been performed for the CdS/HgS QDQW. The parameters for this system are the same as those described in the previous section. In figure 3 we can see that the impurity binding energy rises as the shell thickness is reduced. It rises further when the core radius is also reduced. The calculations are done for given dot sizes with varying well thickness. As the well thickness is reduced, the impurity wavefunction gets more confined and as a result becomes deeper. This leads to the rise in the binding energy. When the dot size is reduced the confinement effect is further increased and that leads to even deeper levels. The impurity Bohr radius plays an important role in determining this feature. CdS has a very small impurity Bohr radius. The other important effect that can be noticed is the fact that the impurity wavefunction is mostly confined in the well. Hence the confinement effect is much larger when the well size is reduced, while it is less affected by the changes in the dot sizes. For an impurity in a QD we have found that the binding energy attains a maximum and then falls as the QD size is reduced. We have termed such shallow–deep behaviour 'SHADE'. In contrast to the shallow–deep transitions (SHADE) observed for impurities in quantum dots, the impurity binding energy rises monotonically for a QDQW.

We have also performed calculations for the off-centre hydrogenic impurity in a CdS/HgS QDQW. In our calculation we have used a QDQW with fixed core size ($R_d = 32$ Å) and an

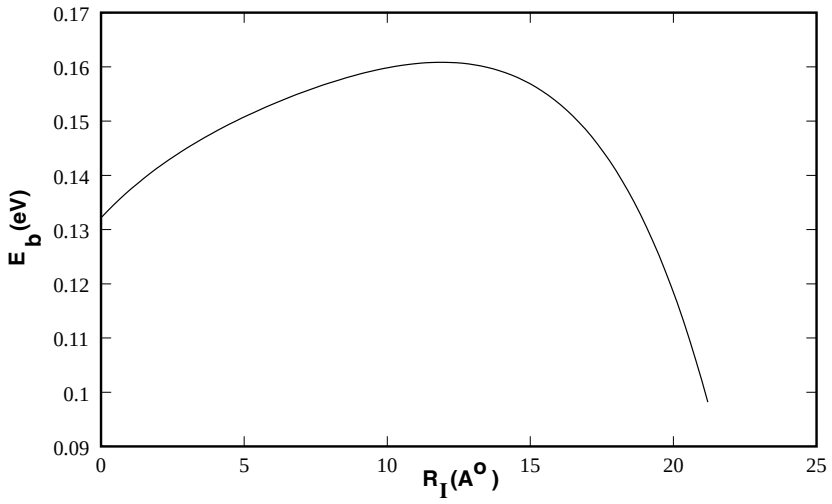

Figure 4. The binding energy of the off-centre hydrogenic impurity in a CdS/HgS QDQW (of fixed size $R_w = 37$ Å) with fixed core size ($R_d = 32$ Å) and well thickness as a function of the impurity position (R_I). The shallow impurity becomes deep when the impurity is moved away from the centre of the QDQW towards the well. As the impurity is moved further outwards, it becomes shallow. An attempt to explain this intriguing shallow–deep (SHADE) transition is made in the text.

overall QDQW size $R_w = 37$ Å. We move the impurity away from the centre of the QDQW and calculate the binding energy of this off-centre impurity as a function of the impurity position within the QDQW. We see in figure 4 that as the impurity is shifted away from the centre, the binding energy becomes deep. This is in contrast to what is seen in QDs. There the binding energy becomes shallow as an impurity is shifted away from the centre [12]. In figure 4 we have shown plots for off-centre impurities for three different core and well sizes in a CdS/HgS QDQW. We can see that the binding energy is 130 meV when the impurity is at the centre of the QDQW and becomes as large as 170 meV when the impurity is shifted away from the centre. As the impurity in a QDQW is shifted further towards the well, the binding energy becomes shallow again. We observe a shallow–deep transition. We proffer a simple explanation for this behaviour based on the analysis of the impurity wavefunction inside the QDQW. When the impurity is at the centre of the QD, the impurity wavefunction is well confined within the QD itself. As it is shifted away from the centre, the wavefunction overlap with the HgS well becomes larger and this leads to the relaxation of this wavefunction inside the well and the lowering of the impurity level. As it is shifted further, the wavefunction starts sensing the well–dielectric barrier. This leads to the confinement of the wavefunction by the QDQW. Hence the impurity level is again upshifted which leads to the small binding energy.

In a recent publication [2] the significance of growing a layer of a semiconductor material within a quantum dot composed of a different material has been discussed. Quantum dots show efficient photoluminescence but surface states play a very important role in these low-dimensional strongly confined systems. Carrier trapping at surface states may lead to poor photoluminescence. Hence it was felt [2] that if a well of a semiconductor material different from that of the QD is grown over the dot, it may lead to more efficient photoluminescence. We have performed a calculation for the ground-state energy of this system. The system can be described as a monolayer of HgS grown within a CdS QD. The monolayer can be treated as a

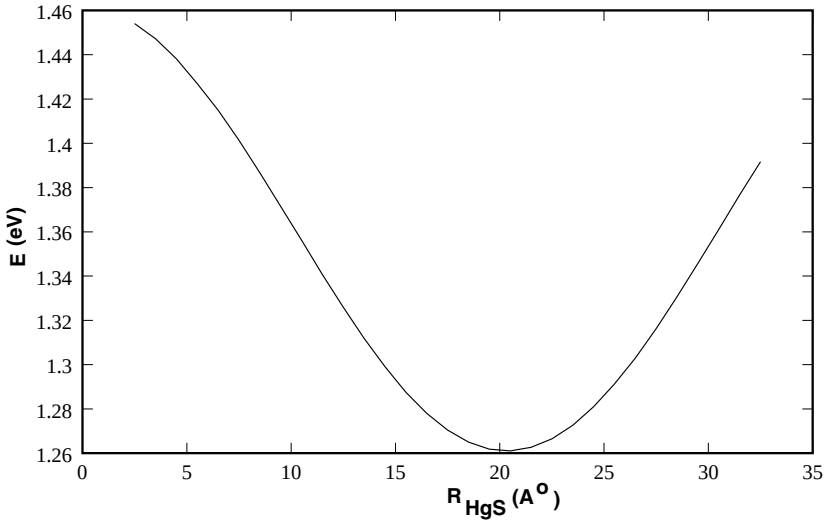

Figure 5. The ground-state energy E of a CdS/HgS QDQW host when the HgS layer is grown in the CdS QD. This is depicted as a function of the HgS layer position inside the CdS core. R_{HgS} is the distance from the centre of the dot to the mid-point of the HgS layer thickness of 5.82 Å. We observe that the ground-state energy goes through a minimum as the HgS layer is dragged from the periphery towards the centre of the spherical system.

'δ-defect' in a QD in analogy with the well known 'δ-doping' in semiconductor literature [27]. We have performed our calculation for the ground-state energy of this system as a function of the position of the HgS monolayer within the QD of a given size. The well is grown not only at the surface of a QD but also inside the QD.

The ground-state energy of the CdS QD of size $R_w = 35$ Å is 1.464 eV. In figure 5 we see that the ground-state energy is downshifted even when a monolayer of HgS (thickness $= 5.82$ Å) is grown at the surface of the CdS QD. When the HgS layer is shifted inward the ground-state energy is further shifted down. The ground-state energy shows a minimum approximately when the HgS layer is in the middle of the QD. When the HgS layer is further shifted towards the centre of the QD, the ground-state energy starts shifting up again. As a result of the HgS layer grown in the CdS QDQW, the probability density in the attractive HgS layer becomes substantial. This leads to a downshift of the ground-state energy. Since the probability density is a maximum towards the middle of the QD, we can expect this effect of lower ground-state energy to be large halfway between the QD centre and the edge. The probability density is again less towards the centre of the QD, the effect is less dominant and we see that the ground-state energy starts rising again. Hence we observe a shallow–deep transition (SHADE) in the QDQW too, as had been noticed earlier in QDs. We can explain this effect by an asymptotic analysis along lines similar to the perturbative analysis developed in the previous section. The only difference is that the perturbation potential is not at the surface but at some point inside the CdS QD of size R_w. It is placed between R_1 and R_2 inside the QD. For this case equation (2.13), above, gets modified to the following:

$$E_p = \frac{2}{R_w}\left[\frac{k^2}{\mu} + V_p\right]\left[\frac{\Delta}{2} - \frac{\sin(2kR_2) - \sin(2kR_1)}{4k}\right] \tag{3.2}$$

with $\Delta = R_2 - R_1$ being the HgS layer thickness and R_w the size of the QDQW. In actual calculations we have taken Δ equal to one monolayer of HgS, i.e. 5.82 Å. We rewrite the last term in the above equation:

$$\frac{\sin(2kR_2) - \sin(2kR_1)}{4k} = \frac{\sin(2k(R_1 + \Delta)) - \sin(2kR_1)}{4k} \approx \frac{\Delta}{2}\cos(2kR_1). \tag{3.3}$$

Substituting equation (3.3) with $R_1 = R_w/2$ in equation (3.2), we get

$$E_p = \frac{2}{R_w}\left[\frac{k^2}{\mu} + V_p\right]\Delta. \tag{3.4}$$

Since the term within the square brackets is negative in this case, this clearly demonstrates that there is a minimum in the ground-state energy when $R_1 = R_w/2$. In figure 5 we see that the ground-state energy can reduce by as much as 0.2 eV. If we include a calculation for the ground-state energy of holes as well as excitonic corrections, then we may expect a substantial reduction in the band gaps of such composite systems, even by the introduction of a mere monolayer of HgS in CdS. Koberling *et al* [2] have claimed in their work a downshift of the absorption onset and emission frequency by almost 1 eV upon embedding a single atomic monolayer of HgS in CdS nanocrystallite. It should be possible to extend their work and verify the non-monotonic behaviour depicted in figure 5.

4. Discussion

Quantum dots (QDs) have opened up new possibilities in the device world. However, surface effects are known to dominate in such nanophase materials. The quantum dot–quantum well system (QDQW) has recently been proposed as an exciting remedial choice for such materials. The field is nascent, being less than a decade old. Starting with the pioneering work of Eychmüller and co-workers [20, 21], the synthesis, characterization, and some linear and non-linear optical properties of QDQW have been studied. It has been shown that the linear absorption of QDQW differs significantly from that of the constituent materials. Thus 'the whole is *not* the sum of the parts'. The band gap can be tuned by core diameter and the well thickness. Haus *et al* [22] demonstrated that the band gap of the composite material depends on both the core and shell radii. Effective-mass theory (EMT) has been used successfully to describe the electronic properties of this system [23–26]. To the best of our knowledge theoretical work on defect states in a QDQW system has not been reported.

We have employed the EMT for all of our calculations. Time and again, the validity of EMT for systems as small as a QD has been questioned. EMT-based calculations over the past decade and a half claim to be in agreement with experiment. Quantum confinement and band upshift in semiconductor nanocrystallites were first predicted on the basis of EMT. More recently it has been claimed that EMT calculations match well with experimental results on QDQWs [23]. We believe that precise quantitative predictions based on EMT cannot be made. On the other hand, our contention is that the essential physics and trends may be extracted from EMT. More importantly, a theoretical consensus can be arrived at by critically examining results based on a variety of methodologies: EMT, the semi-empirical linear combination of atomic orbitals (LCAO), and the local density approximation (LDA).

There are at least two results in this paper which can be verified by experiments. Figure 2 indicates that the curvature of the upshift in a QDQW is opposite to that in a QD. Figure 5 suggests the existence of a minimum as the HgS quantum well is dragged from the periphery of the CdS quantum dot. In fact certain experimental observations [2] provided the motivation for the work leading to figure 5. We have labelled the system described in this figure a δ-defect QDQW. Band-gap engineering has been discussed by workers in the

context of alloy and low-dimensional semiconductor structure [32]. In the context of our work on the δ-defect (figure 5) we suggest a novel type of '*defect engineering*' for semiconductor nanostructures.

Our work should be extended in several ways. Excited states of the hydrogenic impurity must be charted in terms of the QDQW size and other parameters. It has been suggested that the complex optical properties of QDQWs cannot be explained on the basis of s states alone [33]. The work on the δ-defect must be extended to cover systems other than HgS. HgS constitutes a 'potential well'. One might examine systems which constitute a 'potential barrier', e.g. HgS/CdS/HgS. In our calculations we have been careful to take into account the difference in effective masses and employed the BenDaniel–Duke boundary condition [28]. In future the polarization effects due to the difference in dielectric constants must also be examined. Work on a parallel methodology, preferably the LCAO, must also be initiated. In this connection we mention that the chalcogen donor in a QD has recently been studied by means of the LCAO [34]. These extensions should be accompanied by appropriate perturbative, asymptotic, and scaling analyses, an aspect that we have adhered to in this work.

The field of defects in semiconductor heterostructures is a nascent area. There are exciting possibilities. The present work suggests some of these possibilities. It outlines the basic fundamentals and provides a frame of reference for discussing the shallow level and other defect states in quantum dot–quantum well systems.

Acknowledgments

This work was supported by the Department of Atomic Energy through the Board of Research in Nuclear Sciences, India. Help given by Moninder Singh Modgil and Rajan Pandey in using *Mathematica* for parts of the derivations is also acknowledged by V Ranjan.

Appendix A. The numerical methodology

We have employed the Runge–Kutta–Fehlberg (RKF) method [35] and checked the result by means of another scheme, namely the predictor–corrector (PC) approach [36]. The RKF method is a self-consistent calculation. We first describe the numerical methodology adopted for solving for the host QDQW. As stated in equation (2.1), the effective-mass Hamiltonian without the impurity is

$$H = -\frac{\hbar^2}{2}\vec{\nabla}\cdot\left(\frac{1}{m^*(\vec{r})}\,\vec{\nabla}\right) + V(\vec{r}). \tag{A.1}$$

There are two layers in the material: a CdS core, surrounded by an HgS layer. The entire combination is surrounded by a dielectric coating, which provides a finite barrier to the charge carrier inside the QDQW. The Hamiltonian now reads

$$H = \begin{cases} -\dfrac{\hbar}{2m_1^*}\nabla^2 + V_1 & r \leqslant R_d \\ -\dfrac{\hbar}{2m_2^*}\nabla^2 & R_d < r \leqslant R_w \\ -\dfrac{\hbar}{2m_e}\nabla^2 + V_2 & r > R_w \end{cases} \tag{A.2}$$

where m_1^*, m_2^*, and m_e are the electron effective mass in CdS, the electron effective mass in HgS, and the free-electron mass, respectively. Other terms in the above equation are described in the text. We have applied the BenDaniel–Duke boundary condition (equation (2.4)) at each interface, i.e. at the CdS–HgS interface and at the HgS–dielectric interface.

For the specific case of our problem, let us take the first of equations (A.2) and demonstrate the application of the RKF method to this case. For the ground state ($l = 0$), the equation in atomic units (defined earlier in the text) will read as

$$\frac{\mathrm{d}^2\psi}{\mathrm{d}r^2} = (V_1 - E)\psi. \tag{A.3}$$

We have solved the problem on a radial one-dimensional grid. We have used a scheme which determines the grid size at each step of the calculation, such that a predefined accuracy in the result is maintained. To attain this, two different orders of the Runge–Kutta method need to be used. Since the Runge–Kutta method is based on intermediate-function evaluation, the Fehlberg scheme facilitates the use of exactly the same intermediate functions for the Runge–Kutta methods of different orders. This makes the task of making such calculations easier. We have used a fourth-order/fifth-order Runge–Kutta method. Given an initial value of the wavefunction ψ_0 and the first derivative of the wavefunction ψ_0' at the initial grid point r_0, the calculation consists in the following steps. First, the following intermediate points between two grid points r_0 and $r_0 + h$ are defined:

$$r_1 = r_0 + \frac{1}{4}h \tag{A.4}$$

$$r_2 = r_0 + \frac{3}{8}h \tag{A.5}$$

$$r_3 = r_0 + \frac{12}{13}h \tag{A.6}$$

$$r_4 = r_0 + h \tag{A.7}$$

$$r_5 = r_0 + \frac{1}{2}h. \tag{A.8}$$

For each of the above points, corresponding wavefunctions ψ are calculated as follows:

$$\psi_1 = \psi_0 + \frac{1}{4}hf_0 \tag{A.9}$$

$$\psi_2 = \psi_0 + h\left[\frac{3}{32}f_0 + \frac{9}{32}f_1\right] \tag{A.10}$$

$$\psi_3 = \psi_0 + h\left[\frac{1932}{2197}f_0 - \frac{7200}{2197}f_1 + \frac{7296}{2197}f_2\right] \tag{A.11}$$

$$\psi_4 = \psi_0 + h\left[\frac{439}{216}f_0 - 8f_1 + \frac{3680}{513}f_2 - \frac{845}{4104}f_3\right] \tag{A.12}$$

$$\psi_5 = \psi_0 + h\left[-\frac{8}{27}f_0 + 2f_1 - \frac{3544}{2565}f_2 + \frac{1859}{4104}f_3 - \frac{11}{40}f_4\right] \tag{A.13}$$

where $f_0,\ f_1,\ f_2,\ f_3$, and f_4 are intermediate functions needed for the calculation using the Runge–Kutta method. The wavefunction derivatives ψ' are calculated at intermediate grid points exactly as the wavefunction ψ is calculated above. The only difference is that we will call the intermediate functions for the ψ'-evaluation $g_0, g_1,\ g_2,\ g_3$, and g_4, to avoid confusion. The intermediate functions are evaluated, in accordance with equation (A.3), as follows:

$$f_i = \psi_i' \tag{A.14}$$

$$g_i = (V_1 - E)\psi_i \tag{A.15}$$

where $i = 0, 1, 2, 3, 4$.

The fourth-order Runge–Kutta expression is given by

$$\psi(r_0 + h) = \psi(r_0) + h\left[\frac{25}{216}f_0 + \frac{1408}{2565}f_2 + \frac{2197}{4104}f_3 - \frac{1}{5}f_4\right] \tag{A.16}$$

and the fifth-order Runge–Kutta expression is given by

$$\hat{\psi}(r_0 + h) = \psi(r_0) + h\left[\frac{16}{135}f_0 + \frac{6656}{12\,825}f_2 + \frac{2856}{56\,430} - \frac{9}{50}f_4 + \frac{2}{55}f_5\right]. \tag{A.17}$$

The same holds for ψ' too. The solution of the differential equation is the one given by the fourth-order formula, whereas the fifth-order equation with the fourth-order equation is used to determine the grid size for the next step of the calculation. The difference between the two solutions obtained is the measure of error. To keep this error at some predetermined level, a new grid size is calculated for the next step and the process is continued up to the last grid point. The grid size in the Fehlberg method is calculated using the following scheme:

$$h_{\text{new}} = h\sqrt[4]{\frac{h\epsilon}{|\psi(r_0 + h) - \hat{\psi}(r_0 + h)|}} \tag{A.18}$$

where h_{new} is the new grid size, h is the previous grid size, and ϵ is the desired accuracy. ψ and $\hat{\psi}$ are the Runge–Kutta fourth-order and fifth-order solutions, respectively, of the Schrödinger equation. The new grid size is calculated after the calculation of both the wavefunction ψ and ψ'. The one which is smaller is accepted for the next step. Hence the grid size for the next step is calculated within the desired accuracy by an inbuilt mechanism in the program.

We first solve the problem with a CdS layer. Then we introduce the HgS well in the problem. This leads to lowering of the eigenvalue obtained earlier. This we find is the faster way of solving the problem. We start the program far outside the QDQW, where we have assumed the wavefunction and its derivative to be zero. The program then runs in several iterations, until it finds a partial wavefunction, which is close to zero at the origin within some predefined accuracy. It accepts this solution, as both of the boundary conditions (that the partial wavefunction has to be zero at the origin and far outside) are satisfied. The same process is repeated for all sizes of the QDQW.

The program is run up to the last grid point before the interface. The wavefunction derivative is then multiplied by the ratio of masses across the interface ($\beta = m_i/m_o$) and the program propagates to the grid point inside the next layer. In this way the BenDaniel–Duke condition (equation (2.4)) is incorporated:

$$\psi'(r_i) = \beta\psi'(r_i) \tag{A.19}$$

where i represents the grid point at the interface.

We have used the Adams–Bashforth–Moulton scheme [36] for the predictor–corrector method that we have used. The grid size is chosen after several runs. It is such that the program converges quickly and gives accurate results. The grid size of $R_w/100$ everywhere except at the interface, where it is chosen to be $R_w/100$, works well for the QDQW sizes under consideration.

Next we introduce an impurity potential $-e^2/\epsilon r$ in the QDQW (see equation (2.1)). A logarithmic mesh is used in order to capture the physics near the impurity centre with fidelity. The numerical approach taken is similar to the one outlined above.

References

[1] Singh M, Ranjan V and Singh V A 2000 *Int. J. Mod. Phys.* B **14** 1753
[2] Koberling F, Mews A and Basche T 1999 *Phys. Rev.* B **60** 1921
[3] Anand S, Carlsson N, Pistol M-E, Samuelson L and Seifert W 1995 *Appl. Phys. Lett.* **67** 3016

[4] Bol A A and Meijerink A 1998 *Phys. Rev.* B **58** R15997
[5] Yan K, Changkui Duan, Yi Ma, Shangda Xia and Krupa J-C 1998 *Phys. Rev.* B **58** 13585
[6] Bastard G 1981 *Phys. Rev.* B **24** 4714
[7] Brown J W and Spector H N 1986 *J. Appl. Phys.* **59** 1179
[8] Weber G, Schultz P A and Oliviera L E 1988 *Phys. Rev.* B **38** 2179
[9] Zhu J L 1989 *Phys. Rev.* B **39** 8780
[10] Chuu D S, Hsiao C M and Mei W N 1992 *Phys. Rev.* B **46** 3898
[11] Porras-Montenegro N and Perez-Merchancano S T 1992 *Phys. Rev.* B **46** 9780
[12] Porras-Montenegro N and Perez-Merchancano S T 1993 *J. Appl. Phys.* **74** 7624
[13] Ribeiro F J and Latge A 1994 *Phys. Rev.* B **50** 4913
[14] Zhu J L, Zhao J H and Xiong J J 1994 *Phys. Rev.* B **50** 1832
[15] Fanyao Q, Fonseca A L A and Nunes O A C 1997 *J. Appl. Phys.* **82** 1236
[16] Zhu J L, Wu J, Fu R T, Chen H and Kawazoe Y 1997 *Phys. Rev.* B **55** 1673
[17] Charrour R, Bouhassoune M, Fliyou M, Bria D and Nougaoui A 2000 *J. Appl. Phys.* **88** 3514
[18] Ranjan V and Singh V A 2001 *J. Appl. Phys.* **89** 6415
[19] Yngve S 1986 *Am. J. Phys.* **54** 1103
[20] Eychmüller A, Mews A and Weller H 1993 *Chem. Phys. Lett.* **208** 59
[21] Mews A, Eychmüller A, Giersig M, Schoos D and Weller H 1994 *J. Phys. Chem.* **98** 934
[22] Haus J W, Zhou H S, Honma I and Komiyama H 1993 *Phys. Rev.* B **47** 1359
[23] Schoos D, Mews A, Eychmüller A and Weller H 1994 *Phys. Rev.* B **49** 17072
[24] Chang K and Xia J-B 1998 *Phys. Rev.* B **57** 9780
[25] Yeh A T, Cerullo G, Banin U, Mews A, Alivisatos A P and Shank C V 1999 *Phys. Rev.* B **59** 4973
[26] Jaskolski W and Bryant G W 1998 *Phys. Rev.* B **57** R4237
[27] Datta S (ed) 1996 *Delta-Doping of Semiconductors* (Cambridge: Cambridge University Press)
[28] BenDaniel D and Duke C 1966 *Phys. Rev.* **152** 683
[29] Wang Y and Herron N 1991 *J. Chem. Phys.* **95** 525
[30] Ogut S, Chelikowsky J and Louie S 1997 *Phys. Rev. Lett.* **79** 1770
[31] Buuren T V, Dinh L N, Chase L L, Siekhaus W J and Terminello L J 1998 *Phys. Rev. Lett.* **80** 3803
[32] Weisbuch C and Winter B 1991 *Quantum Semiconductor Structures* (Boston, MA: Academic)
[33] Mews A and Eychmüller A 1998 *Ber. Bunsenges. Phys. Chem.* **102** 1343
[34] Ranjan V, Singh V A and Kapoor M 2000 *Physics of Semiconductor Devices* ed V Kumar and S K Agarwal (New Delhi: Allied)
[35] DeVries P L 1994 *A First Course in Computational Physics* (New York: Wiley)
[36] Press W H, Teukolsky S A, Vetterling W T and Flannery B P 1995 *Numerical Recipes in C* (Delhi: Cambridge University Press)